Biosensors and Bioelectronics 210 (2022) 114299

Contents lists available at ScienceDirect

Biosensors and Bioelectronics

journal homepage: www.elsevier.com/locate/bios

Assessment of fibrinolytic status in whole blood using a dielectric coagulometry microsensor

Sina Pourang [a], Ujjal D.S. Sekhon [b], Dante Disharoon [b], Sanjay P. Ahuja [c], Michael A. Suster [a], Anirban Sen Gupta [b,**], Pedram Mohseni [a,b,*]

[a] Department of Electrical, Computer, and Systems Engineering, Case Western Reserve University, Cleveland, OH, 44106, USA
[b] Department of Biomedical Engineering, Case Western Reserve University, Cleveland, OH, 44106, USA
[c] Division of Pediatric Hematology/Oncology, Rainbow Babies and Children's Hospital, Case Western Reserve University, Cleveland, OH, 44106, USA

ARTICLE INFO

Keywords:
Dielectric coagulometry
Dielectric spectroscopy
Fibrinolysis monitoring
Microfluidics
Point-of-care diagnostics
Whole blood coagulation

ABSTRACT

Rapid assessment of the fibrinolytic status in whole blood at the point-of-care/point-of-injury (POC/POI) is clinically important to guide timely management of uncontrolled bleeding in patients suffering from hyperfibrinolysis after a traumatic injury. In this work, we present a three-dimensional, parallel-plate, capacitive sensor – termed ClotChip – that measures the temporal variation in the real part of blood dielectric permittivity at 1 MHz as the sample undergoes coagulation within a microfluidic channel with <10 μL of total volume. The ClotChip sensor features two distinct readout parameters, namely, lysis time (LT) and maximum lysis rate (MLR) that are shown to be sensitive to the fibrinolytic status in whole blood. Specifically, LT identifies the time that it takes from the onset of coagulation for the fibrin clot to mostly dissolve in the blood sample during fibrinolysis, whereas MLR captures the rate of fibrin clot lysis. Our findings are validated through correlative measurements with a rotational thromboelastometry (ROTEM) assay of clot viscoelasticity, qualitative/quantitative assessments of clot stability, and scanning electron microscope imaging of clot ultrastructural changes, all in a tissue plasminogen activator (tPA)-induced fibrinolytic environment. Moreover, we demonstrate the ClotChip sensor ability to detect the hemostatic rescue that occurs when the tPA-induced upregulated fibrinolysis is inhibited by addition of tranexamic acid (TXA) – a potent antifibrinolytic drug. This work demonstrates the potential of ClotChip as a diagnostic platform for rapid POC/POI assessment of fibrinolysis-related hemostatic abnormalities in whole blood to guide therapy.

1. Introduction

Hemostasis is a delicate equilibrium between clot formation – characterized by the development of a platelet plug and concomitant deposition of a fibrin mesh – and clot resolution, which is regulated by the fibrinolytic system that limits clot growth to prevent thrombotic occlusions. Events such as liver transplantation, vascular surgery, or traumatic injury can render an imbalance in hemostasis and lead to coagulopathy (Kornblith et al., 2019). For example, hyperfibrinolysis is a prominent and lethal form of coagulopathy, occurring in 18% of severe trauma patients (Moore et al., 2014) and carrying a mortality rate of 40–75% (Cotton et al., 2012; Moore et al., 2014). During hyperfibrinolysis, the fibrinolytic system becomes upregulated and counteracts the formation of a stable fibrin clot, leading to uncontrolled bleeding. This occurs through two parallel pathways. First, blood loss following injury results in hypoxic tissue shock and subsequent increased secretion of tissue plasminogen activator (tPA) from the injured vascular endothelium, which locally converts plasminogen to the fibrinolytic enzyme plasmin (Chapman et al., 2016). Second, hypoperfusion induces endothelial thrombomodulin expression leading to the activation of protein C, which in turn depletes plasminogen activator inhibitor 1 (PAI-1) (Brohi et al., 2007). Since PAI-1 is the most prevalent endogenous inhibitor of tPA, both of these pathways ultimately manifest as systemically elevated tPA levels. Clinical trials in bleeding trauma patients have demonstrated that the antifibrinolytic agent tranexamic acid (TXA), which blocks tPA-dependent plasmin generation, can improve outcomes for patients suffering from hyperfibrinolysis, but only if administered within a narrow time window of 3 h

* Corresponding author. Department of Electrical, Computer, and Systems Engineering, Case Western Reserve University, Cleveland, OH, 44106, USA.
** Corresponding author.
E-mail addresses: axs262@case.edu (A. Sen Gupta), pxm89@case.edu (P. Mohseni).

https://doi.org/10.1016/j.bios.2022.114299
Received 20 February 2022; Received in revised form 12 April 2022; Accepted 19 April 2022
Available online 26 April 2022
0956-5663/© 2022 Elsevier B.V. All rights reserved.

after the onset of bleeding (Roberts et al., 2013). Hence, rapid diagnosis of hyperfibrinolysis after a traumatic injury is critical to guide timely patient care at the point-of-care/point-of-injury (POC/POI).

Standard coagulation assays used to diagnose coagulopathy either do not screen for hyperfibrinolysis or are logistically challenging to be performed within the therapeutic time window especially at POC/POI. For example, plasma-based laboratory tests such as activated partial thromboplastin time (aPTT) and prothrombin time/international normalized ratio (PT/INR) cannot independently detect hyperfibrinolysis (Kutcher et al., 2012). Euglobulin lysis time (ELT) is another plasma-based test that does screen for hyperfibrinolysis, but is not well suited for clinical settings and requires 2–3 h to perform (Katz et al., 1970).

An alternative to plasma-based coagulation assays is whole blood-based viscoelastic measurements performed by thromboelastography (TEG) and rotational thromboelastometry (ROTEM), which can provide a global assessment of the hemostatic system, including the state of fibrinolysis (Brill et al., 2021). However, TEG/ROTEM are bulky, expensive, unavailable outside of well-equipped hospital settings, require specialized personnel to operate, and cannot be easily transported for use at POC/POI (Hartmann et al., 2020).

Recently, microfluidic devices along with microfabricated or printed sensors have been developed with the potential to offer timely assessments of hemostatic function at POC/POI using small blood sample volumes (Mohammadi Aria et al., 2019; Diamond and Rossi, 2021). Specifically, a wide range of technologies have been developed to monitor the blood coagulation dynamics using various transduction and readout strategies such as flow imaging (Sweeney et al., 2019), velocity/deformation imaging (Li et al., 2022), electrical impedance measurement (Ramaswamy et al., 2013; Lei et al., 2013; Li et al., 2019; Williams et al., 2021), microcantilevers oscillation (Cakmak et al., 2015), surface acoustic waves (Harder et al., 2019), and film bulk acoustic resonance (Chen et al., 2017). However, these devices characterize the overall coagulation status only and do not provide specific information on platelet function or the fibrinolytic system. To partially address such limitations, researchers have developed microfluidic hemostatic models that are sensitive to both the coagulation system and platelet function (Schoeman et al., 2017), as well as flow-based microfluidic devices to investigate platelet thrombus formation (Xu et al., 2020) or monitor whole blood hemostasis and platelet function (Jain et al., 2016; Rossi and Diamond, 2020). However, these approaches do not assess the fibrinolytic system.

A more readily translatable approach is to eliminate the complexity of flow-based operation by monitoring μL-range whole blood samples in stasis mode within a microfluidic channel using the electronic technique of dielectric spectroscopy (DS). DS measurements of coagulating blood in the MHz-frequency range are shown to be sensitive to the aggregation of red blood cells (RBCs) into a fibrin clot and their subsequent deformation due to contractile forces from activated platelets through the interfacial polarization of RBC membranes (Asami and Sekine, 2007; Hayashi et al., 2008). Hence, dielectric coagulometry can provide comprehensive information on whole blood coagulation status by measuring the temporal variation in the dielectric permittivity of the blood sample at MHz-frequency range as it undergoes coagulation (Hayashi et al., 2010, 2015).

To that end, researchers have recently reported on the simultaneous evaluation of coagulation function, platelet function/count, and hematocrit level via capacitive measurements at 1.3 MHz using a carbon nanotube-paper composite capacitance sensor (Sekar et al., 2022). Furthermore, our team has also previously reported on a microfluidic dielectric sensor – termed ClotChip – for rapid, comprehensive assessment of blood coagulation dynamics by capturing the temporal variation in the blood dielectric permittivity at 1 MHz (Maji et al., 2017). ClotChip is a whole-blood, electronic, label-free assay that obviates the need for laborious, time-consuming steps for sample preparation, e.g., centrifugation/plasma separation and fluorescence/magnetic tagging. Through three distinct readout parameters and using only <10 μL of whole blood, the sensor is shown to provide useful information on the coagulation function, platelet function/count, and fibrin polymerization (Maji et al., 2018; Maji et al., 2019a,b; Pourang et al., 2020; Maji et al., 2021; Pourang et al., 2021).

In this work, for the first time, we introduce two new ClotChip readout parameters, which are shown to provide specific information on the fibrinolytic status of whole blood. This was established through (i) correlative measurements with a ROTEM assay, (ii) qualitative and quantitative assessments of the fibrin clot stability, and (iii) visualizing the clot ultrastructural changes using scanning electron microscope (SEM) imaging, all in a tPA-induced fibrinolytic environment. Finally, we will also establish the ClotChip ability to detect the effects of TXA on inhibiting tPA-induced upregulated fibrinolysis, leading to the rescue of normal hemostatic function.

2. Material and methods

2.1. ClotChip structure, fabrication, and testing procedure

The ClotChip structure was based on a three-dimensional (3D), parallel-plate, capacitive sensor embedded within a microfluidic channel to extract the dielectric permittivity of whole blood in stasis mode (Maji et al., 2017). As seen in Fig. 1A, the sensor comprised three layers including two polymethyl methacrylate (PMMA) plastic substrates and one double-sided-adhesive (DSA) film. The PMMA substrates housed two planar sensing electrodes and one floating electrode that were separated from each other through a microfluidic channel formed by laser-micromachining the DSA film. The sensor was assembled by aligning and attaching the two PMMA substrates together using the DSA film as shown in Fig. 1B. With a blood sample placed within the 3D, capacitive, sensing area, the impedance of the sensor would change based on the blood dielectric permittivity (Maji et al., 2017).

Fig. 1C depicts the ClotChip fabrication steps and its measurement procedure. First, a 1.5 mm-thick PMMA sheet (McMaster-Carr, Robbinsville, NJ) was laser-cut (Versa Laser 2.3, Universal Laser Systems Inc., Scottsdale, AZ) into a 10 cm × 10 cm-substrate to fit onto the substrate holder of an MPM TF-100 thick-film printer with a 325 mesh screen, which was capable of a minimum line width/spacing of 150 μm. Prior to printing the electrodes on it, the substrate was cleaned with 70% isopropyl alcohol and dried under nitrogen flow. The sensing electrodes (3.5 mm × 1.3 mm with spacing of 0.5 mm) and the floating electrode (4 mm × 1.5 mm) were printed using gold ink (E4464, Ercon Inc., Wareham, MA) and baked for 20 min at 100 °C in an oven to dry. The electrodes were designed with a minimum line width of 1.3 mm and a minimum spacing of 0.5 mm, which were >8 × and >3 × the minimum achievable levels, respectively, to enable reproducible manufacture of prototype sensors using low-cost equipment. Next, the PMMA substrate containing the printed electrodes and the 250 μm-thick DSA film (Digikey, Thief River Falls, MN) were laser-micromachined to create the individual ClotChip sensor layers shown in Fig. 1A. For sensor assembly, the two PMMA substrates were pre-cleaned with 70% ethanol and then aligned by hand. The dimensions of the electrodes were designed to allow for the 3D, capacitive, sensing area (defined by the overlap of the sensing and floating electrodes) to remain constant for up to ~1 mm of misalignment. A fully assembled sensor measured 26 mm × 9 mm × 3 mm, with a total sample volume of <10 μL in the microfluidic channel.

Before conducting ClotChip measurements and to induce coagulation, 25.6 μL of $CaCl_2$ (250 mM) was pipetted into 300 μL of citrated whole blood sample pre-warmed to 37 °C. Next, 9 μL of the mixture was immediately injected into the ClotChip microfluidic channel that was pre-washed with 30% ethanol and rinsed three times with phosphate-buffered saline (PBS) prior to sample loading. The dielectric permittivity of the blood sample was then measured in a frequency range of 10 kHz–100 MHz (see representative curves in Supplementary Fig. S1) using an impedance analyzer (Agilent 4294A, Santa Clara, CA) that was

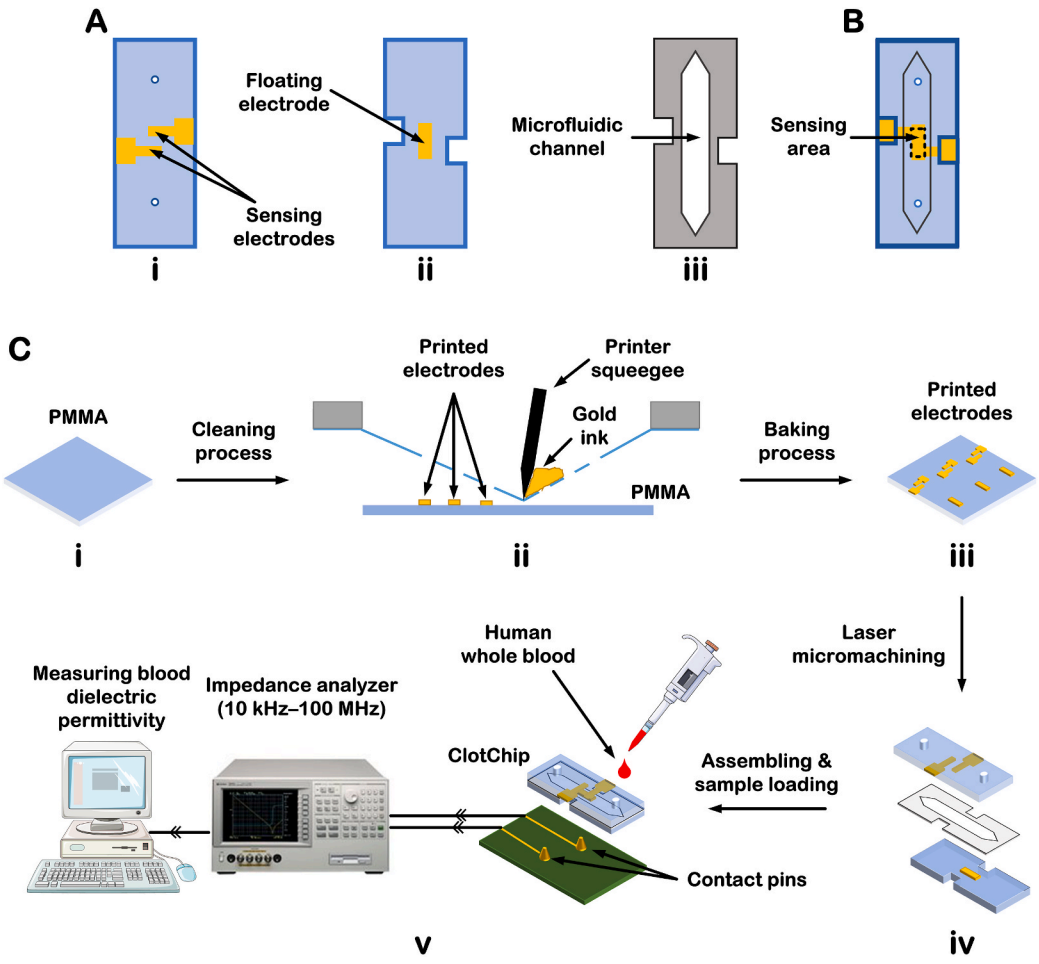

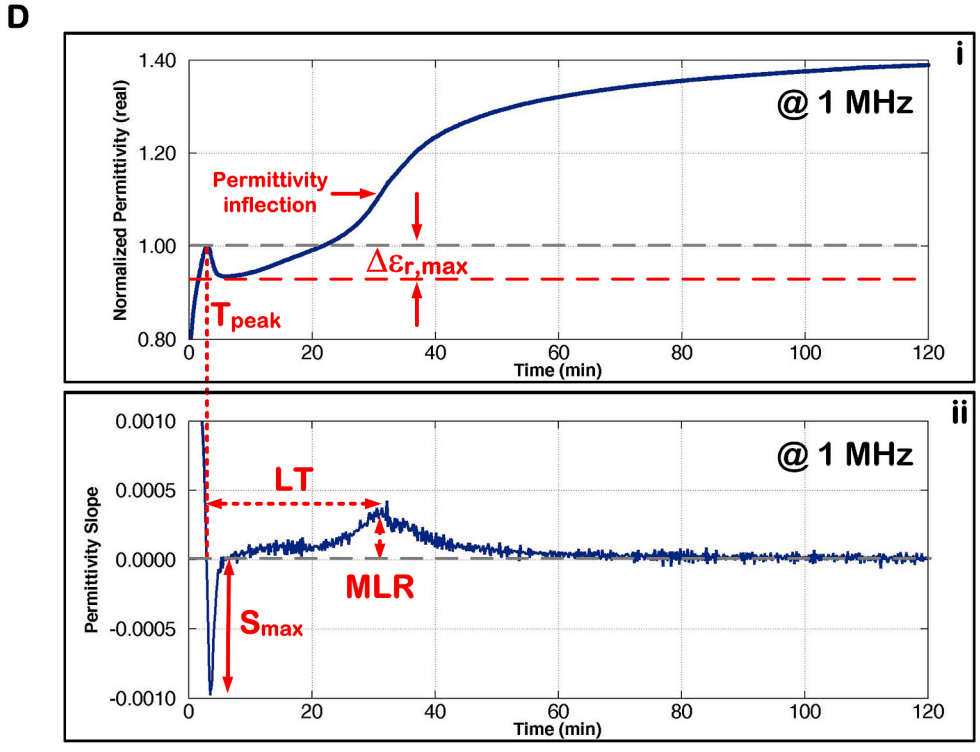

Fig. 1. ClotChip structure, fabrication, and testing. **A)** Illustration of the three sensor's layers including two polymethyl methacrylate (PMMA) plastic substrates with (i) sensing and (ii) floating gold electrodes, as well as (iii) a double-sided-adhesive (DSA) film with thickness of 250 μm that was laser-micromachined to form the walls of a microfluidic channel. **B)** Assembled ClotChip sensor after attaching the two PMMA layers together using the DSA film. The total sample volume in the microfluidic channel was <10 μL. **C)** Illustration of ClotChip fabrication steps and testing procedure. (i–ii) The gold sensing and floating electrodes were screen-printed onto a single pre-cleaned PMMA plastic substrate using a thick-film printer. (iii–iv) The PMMA substrate was baked in an oven to dry the printed electrodes and then laser-micromachined (along with the DSA film) to create the individual ClotChip sensor layers as shown in **A**. (v) Assembled ClotChip sensor was loaded with human whole blood and interfaced with an impedance analyzer for measurements of the blood dielectric permittivity in a frequency range of 10 kHz–100 MHz. **D)** Example of the ClotChip readout curve and related parameters for a human whole blood sample undergoing coagulation in a tissue plasminogen activator (tPA)-induced fibrinolytic environment. (i) T_{peak} and $\Delta\varepsilon_{r,max}$ were derived from the normalized real part of blood dielectric permittivity at 1 MHz. (ii) S_{max}, lysis time (LT), and maximum lysis rate (MLR) were derived from the first derivative of the readout curve (i.e., permittivity slope).

electrically connected to the ClotChip sensing electrodes through contact openings in the bottom PMMA substrate (and DSA film) using spring-loaded contact pins. Duplicate ClotChip measurements were performed every 10 s over a total measurement time of 120 min, with the setup kept at 37 °C inside a thermostatic chamber (Thermolyne, Dubuque, IA).

2.2. Blood sample procurement and in vitro treatment

De-identified human whole blood samples were drawn by venipuncture into standard collection tubes containing 3.2% sodium citrate anticoagulant from healthy volunteers at the Hematopoietic Biorepository and Cellular Therapy Core at Case Western Reserve University under an institutional review board (IRB)-approved protocol. The

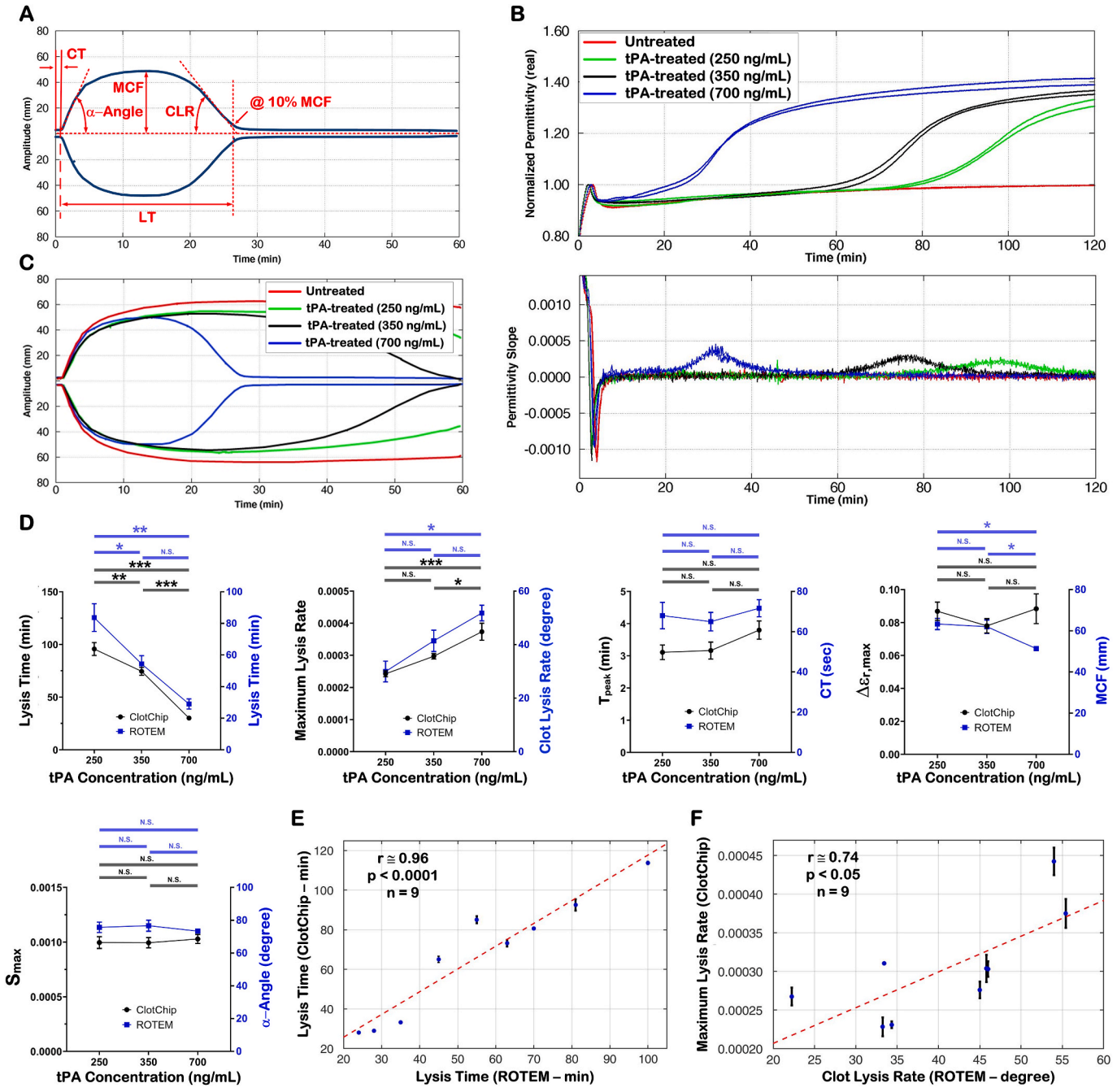

Fig. 2. ClotChip and rotational thromboelastometry (ROTEM) parameters in a fibrinolytic environment. **A)** Example of the ROTEM profile and related parameters for a human whole blood sample undergoing coagulation in a tPA-induced fibrinolytic environment. **B)** ClotChip readout curve and its first derivative for an untreated whole blood sample as well as samples treated with three different concentrations of tPA. All samples had tissue factor (TF) added to them at a concentration of 1 pg/mL. **C)** ROTEM profiles obtained for the four blood samples used in **B**. **D)** Variation of ClotChip and ROTEM parameters with different tPA concentrations. The lysis time (LT) parameter of both assays showed significant sensitivity to tPA concentrations, with the LT parameter decreasing as tPA concentrations increased. Similarly, the ClotChip maximum lysis rate (MLR) and ROTEM clot lysis rate (CLR) parameters exhibited sensitivity to tPA concentrations, with both parameters increasing as tPA concentrations increased. Error bars are presented as mean ± standard error of mean (SEM) of six ClotChip and three ROTEM measurements for each tPA concentration. **E)** A very strong positive correlation ($r \cong 0.96$, $p < 0.0001$, $n = 9$) was observed between the LT parameters of ClotChip and ROTEM assays. **F)** A strong positive correlation ($r \cong 0.74$, $p < 0.05$, $n = 9$) was observed between the ClotChip MLR and ROTEM CLR parameters. Error bars in **E–F** are presented as mean ± SEM of duplicate ClotChip measurements.

blood samples were stored at room temperature and tested within 2 h of collection.

In some tests, the samples were treated *in vitro* to induce dysregulated fibrinolysis and to subsequently correct the hemostatic function. Specifically, tPA (Sigma-Aldrich, St Louis, MO) was added to the blood samples at various concentrations to degrade fibrin into fibrin degradation products via the activation of plasminogen into plasmin. The lyophilized tPA was reconstituted in de-ionized (DI) water at a concentration of 1 mg/mL based on manufacturer's instructions, immediately aliquoted, frozen, and kept at −20 °C. In other tests, TXA (Sigma-Aldrich, St Louis, MO) at two different concentrations was added to the tPA-treated blood samples to inhibit dysregulated fibrinolysis and correct the hemostatic function. Finally, a reagent containing tissue factor (TF) (ROTEM EXTEM reagent, Instrumentation Laboratory, Bedford, MA) was diluted and added to all samples with a final TF concentration of 1 pg/mL as measured by an ELISA kit (Abcam, Cambridge, MA).

2.3. ClotChip readout curve in a fibrinolytic environment

The ClotChip readout curve was defined as the temporal variation in the normalized real part of blood dielectric permittivity at 1 MHz as the sample was undergoing coagulation (Maji et al., 2017). Fig. 1D shows a representative ClotChip readout curve and its first derivative (i.e., permittivity slope) for a human whole blood sample undergoing coagulation in a tPA-induced fibrinolytic environment. We have previously identified three readout parameters, namely, T_{peak}, $\Delta\varepsilon_{r,max}$, and S_{max}, which are, respectively, sensitive to the detection of clotting defects at the non-cellular level (i.e., coagulation factor) (Maji et al., 2018, 2019a, 2021), cellular level (i.e., platelet) (Maji et al., 2017, 2018, 2019b), and in fibrin polymerization (Pourang et al., 2020), and the impact of such abnormalities on the overall hemostatic status of whole blood. In this work, we introduce two new ClotChip readout parameters, namely, lysis time (LT) and maximum lysis rate (MLR) as depicted in Fig. 1D, which can provide new information on the fibrinolytic status of whole blood. Specifically, LT is defined as the time interval between T_{peak} and the fibrinolysis-induced inflection point on the tail end of the readout curve, whereas MLR captures the rate of such inflection.

2.4. Hemostatic assessment with a ROTEM viscoelastic assay

Measurements were performed to establish the correlative power of the ClotChip sensor to ROTEM – a clinically relevant, viscoelastic, whole-blood assay of global hemostasis (Hartmann et al., 2020). Specifically, following the manufacturer's directions, a quad-channel computerized ROTEM Coagulation Analyzer (ROTEM Delta, TEM International, Munich, Germany) was used with the EXTEM assay in which coagulation was initiated by TF. Fig. 2A shows a representative ROTEM profile for a human whole blood sample undergoing coagulation in a tPA-induced fibrinolytic environment. The curve features multiple readout parameters that provide important information on all aspects of blood coagulation process. We have previously established a strong positive correlation between the ClotChip T_{peak}, $\Delta\varepsilon_{r,max}$, and S_{max} parameters and, respectively, the ROTEM clotting time (CT), maximum clot firmness (MCF), and α-angle parameters (Maji et al., 2017, 2019a; Pourang et al., 2020).

The ROTEM lysis time (LT) and clot lysis rate (CLR) parameters provide information about the fibrin clot lysis. As shown in Fig. 2A, LT (in sec) is defined as the time from CT until the clot firmness is decreased to 10% of MCF during fibrinolysis, whereas CLR (in degree) is defined as the angle between the baseline and the tangent to the declining clot firmness curve (Görlinger et al., 2021). In this work, we have assessed the correlation of ClotChip LT and MLR parameters to the ROTEM LT and CLR parameters, respectively, by conducting concurrent measurements on the same tPA-treated whole blood samples. ROTEM measurements lasted 120 min and were performed within 2 h of the time of blood collection. ROTEM profiles were plotted for the first 60 min of the measurement time.

2.5. Fibrin clot stability assessment with hemoglobin measurements

Measurements of hemoglobin (Hb) concentrations at three pre-defined time points were performed for a quantitative assessment of the stability of fibrin clots inside the ClotChip microfluidic channel. The rationale was that the fibrin clot lysis would release the RBCs trapped in the clot, the extent of which can then be quantified by measuring Hb content of the RBCs. Hemoglobin analysis was performed using the sodium lauryl sulphate (SLS) method (Oshiro et al., 1982), which involved mixing the blood samples with the SLS solution, transferring the mixtures to well plates, and reading the amount of light absorbance (at a wavelength of 539 nm) via a microplate reader. To prepare the mixtures, 100 μL of PBS was injected into the ClotChip microfluidic channel at each pre-defined time point. Next, 5 μL of the sample was collected from the channel with a pipette, transferred into a microtube, and mixed with 1 mL of SLS solution at a concentration of 2.08 mM (buffered to a pH level of 7.2). A visual observation of fibrin clots inside the ClotChip microfluidic channel was also performed after PBS injection at each pre-defined time point for a qualitative assessment of clot stability.

2.6. Blood sample preparation for scanning electron microscope imaging

Sample-preparation procedure for SEM imaging comprised two stages of fixing and dehydration. The first stage was initiated by fixing the blood samples with 2.5% glutaraldehyde (Sigma-Aldrich, St Louis, MO) in PBS (pH of 7.4) for 1 h. This continued with 1% osmium tetroxide (OsO_4, Sigma-Aldrich, St Louis, MO) in DI water for 1 h, followed by 1% thiocarbohydrazide (Sigma-Aldrich, St Louis, MO) in DI water for 5 min and 1% OsO_4 again for 5 min. The samples were washed thrice with PBS for 5 min in between each step. Some samples were also centrifuged (at 500 g for 5 min) in between each step to remove fixer reagents, if needed.

The dehydration stage was initiated by serially rinsing the samples seven times in DI water-diluted ethanol (30%, 40%, 50%, …., 90%) and two times with 100% ethanol, each for 10 min. This was next followed by impregnation with 50% hexamethyldisilazane (HMDS) (Sigma-Aldrich, St Louis, MO) in ethanol for 20 min. Finally, 100% HMDS was added to the dried samples, which were then air-dried overnight at room temperature, mounted, coated with 15-nm gold, and imaged with an FEI Helios-FIB SEM at 1 kV.

2.7. Statistical analysis

The data obtained in this study are reported as mean ± standard error of mean (SEM). The data were analyzed using one-way analysis of variance (ANOVA) with Tukey's post hoc test for multiple comparisons, with the statistical significance threshold set at 95% confidence level for all tests ($p < 0.05$). The degree of statistical significance is marked with * for $0.01 < p < 0.05$, ** for $0.001 < p < 0.01$, and *** for $p < 0.001$. A p value exceeding 0.05 is marked as N.S. (Not Significant). Statistical analyses were performed with GraphPad Prism (GraphPad Software, La Jolla, CA) software suite. Pearson's correlation was used to obtain correlative statistics between the readout parameters of the ClotChip and ROTEM assays.

3. Results

3.1. ClotChip and ROTEM parameters in a fibrinolytic environment

Fig. 2B shows the ClotChip readout curve and its first derivative for an untreated whole blood sample as well as samples treated *in vitro* with three different tPA concentrations of 250, 350, and 700 ng/mL. These levels are on the lower end of tPA concentration range used to induce upregulated fibrinolysis during *in vitro* studies (Picetti et al., 2019).

While the tail end of the curve remained relatively flat for the untreated sample, the tail ends of the curves for the three tPA-treated samples exhibited a characteristic inflection point and subsequent rise in permittivity in a tPA dose-dependent manner.

The ClotChip readout parameters, including LT and MLR, associated with each tPA concentration were then obtained from these measurements. The corresponding ROTEM profiles for these four blood samples are also shown in Fig. 2C, which in turn yielded the ROTEM readout parameters associated with each tPA concentration.

Fig. 2D depicts the variation of all these readout parameters with different tPA concentrations in a fibrinolytic environment. As can be seen, the ClotChip T_{peak}, $\Delta\varepsilon_{r,max}$, and S_{max} parameters as well as the ROTEM CT, MCF, and α-angle parameters in general did not exhibit significant variation with tPA concentrations, signifying that clot initiation and clot growth were unaffected by the various tPA conditions. In sharp contrast, the LT parameter of both assays showed significant sensitivity to tPA concentrations, with LT decreasing as tPA concentrations increased. Moreover, the ClotChip MLR and ROTEM CLR parameters also showed sensitivity to tPA concentrations, with both parameters increasing as tPA concentrations increased, indicating a higher rate of fibrin clot lysis.

The ClotChip LT parameter exhibited a very strong positive correlation ($r \cong 0.96$, $p < 0.0001$, $n = 9$) to the ROTEM LT parameter as shown in Fig. 2E, and the ClotChip MLR parameter showed a strong positive correlation ($r \cong 0.74$, $p < 0.05$, $n = 9$) to the ROTEM CLR parameter as shown in Fig. 2F.

3.2. Qualitative and quantitative assessments of fibrin clot stability

As described previously in Section 2.5, visual observation of fibrin clots and measurements of Hb concentrations were performed at pre-defined time points for, respectively, qualitative and quantitative assessments of clot stability inside the ClotChip microfluidic channel. The objective was to examine whether clot morphological status in a fibrinolytic environment was reflected in the temporal pattern of blood permittivity variation or not. Specifically, Fig. 3A shows the ClotChip readout curve and its first derivative for an untreated and a tPA-treated (concentration of 350 ng/mL) whole blood sample. The fibrin clot stability was assessed at three different time points indicated in Fig. 3A corresponding to (i) when permittivity variation after T_{peak} had largely stabilized, (ii) fibrinolysis-induced permittivity inflection point on the tail end of the curve, and (iii) measurement endpoint. Fig. 3B illustrates the methodology used for clot stability assessments, which was also described in detail in Section 2.5.

Fig. 3C shows results from the visual observation of fibrin clots inside the ClotChip microfluidic channel at the three pre-defined time points after PBS injection. The tPA-treated (fibrinolytic) sample showed a stable clot at the first time point, with PBS unable to enter the microfluidic channel from the inlet port. By the time point of permittivity inflection, the fibrin clot had mostly dissolved and washed away after PBS injection. By the measurement endpoint, the microfluidic channel was devoid of any blood. For the latter two time points, all 100 μL of PBS was able to enter the microfluidic channel from the inlet port (and exit from the outlet port). In contrast, the untreated (control) sample formed and maintained a stable clot throughout the 2-h duration of this test, with no sign of the clot dissolving and washing away after PBS injection.

Our visual observations were further confirmed by corresponding measurements of Hb concentrations as depicted in Fig. 3D. Specifically, at the first time point, the Hb concentration of the fibrinolytic sample was at the same level as that of the untreated sample. However, the Hb concentration significantly decreased in the fibrinolytic sample by the permittivity inflection point (and the measurement endpoint), indicating that the fibrin clot had largely dissolved and washed away. On the other hand, the Hb concentration of the untreated (control) sample remained the same at all three time points, indicating the formation of a stable fibrin clot in the absence of tPA.

3.3. SEM images of fibrin clots in a fibrinolytic environment

As described previously in Section 2.6, SEM images of blood samples were obtained to visualize the changes in fibrin clot ultrastructure at the three pre-defined time points on the ClotChip readout curve. Specifically, images of fibrin clots were obtained for an untreated and a tPA-treated (concentration of 350 ng/mL) whole blood sample. Fig. 4 shows the SEM images in which the arrows point to the presence of the fibrin mesh (white) as well as examples of biconcave disk-like RBCs (green) and severely deformed RBCs (red).

Both samples formed stable clots initially as indicated by the deformation of RBCs and their trapping in a netted fibrin mesh by the first pre-defined time point at which the permittivity variation had largely stabilized (plots A–B). By the time point of permittivity inflection, the fibrin mesh had broken down in the fibrinolytic sample due to tPA-induced upregulated fibrinolysis, with the RBCs largely retrieving their biconcave disk-like shape. These changes were not observed in the control sample (plots C–D). By the measurement endpoint, the fibrin mesh had fully dissolved in the fibrinolytic sample, whereas the control sample maintained a stable clot with the continued presence of a dense fibrin mesh and deformed RBCs (plots E–F).

Taken together, the SEM imaging results along with those from qualitative/quantitative clot stability assessments and from correlative ROTEM measurements clearly established that the permittivity inflection point on the tail end of the ClotChip readout curve provides information about the fibrinolytic status of whole blood. Specifically, the ClotChip LT parameter identifies the time that it takes from the onset of coagulation (indicated by T_{peak}) for the fibrin mesh to mostly dissolve in the blood sample during fibrinolysis. The ClotChip MLR parameter captures the rate of fibrin clot lysis, with a higher MLR parameter resulting from a higher tPA concentration.

3.4. Assessment of upregulated fibrinolysis inhibition with ClotChip

After establishing that the ClotChip sensor was sensitive to the detection of upregulated fibrinolysis in whole blood, a final set of experiments was performed to investigate whether the sensor was capable of detecting the correction/rescue in hemostatic function mediated by TXA – a potent antifibrinolytic drug. Fig. 5A shows the ClotChip readout curve and its first derivative for an untreated whole blood sample, a fibrinolytic sample treated with tPA at a concentration of 350 ng/mL, and the same tPA-treated sample with the addition of TXA *in vitro* at two different concentrations of 10 and 15 mg/L. These levels are at each end of TXA concentration range recommended to substantially inhibit tPA-induced upregulated fibrinolysis (Picetti et al., 2019). As can be seen, the fibrinolytic sample once again exhibited a characteristic inflection point on the tail end of the readout curve followed by a rise in permittivity. However, the two TXA-treated samples yielded readout curves that closely resembled that of the untreated sample with no such inflection point present.

The corresponding ClotChip LT and MLR parameters are depicted in Fig. 5B and C, respectively. In the absence of fibrin clot lysis within the 2-h duration of these experiments for the untreated and TXA-treated samples, a value of 120 min was assigned to LT for plotting the data. With the addition of TXA to the tPA-treated samples, there was a significant increase in LT and a significant decrease in MLR parameters, indicating that the ClotChip sensor could detect the resistance to clot lysis (correction in hemostatic function) that occurred with TXA addition. Finally, Supplementary Fig. S2 shows representative SEM images of fibrin clots obtained at the measurement endpoint for two whole blood samples treated with tPA (350 ng/mL) and TXA (10 and 15 mg/L). As expected, similar to an untreated sample (see Fig. 4), both samples had still maintained stable clots at the measurement endpoint as evident by the presence of a dense fibrin mesh and deformed RBCs.

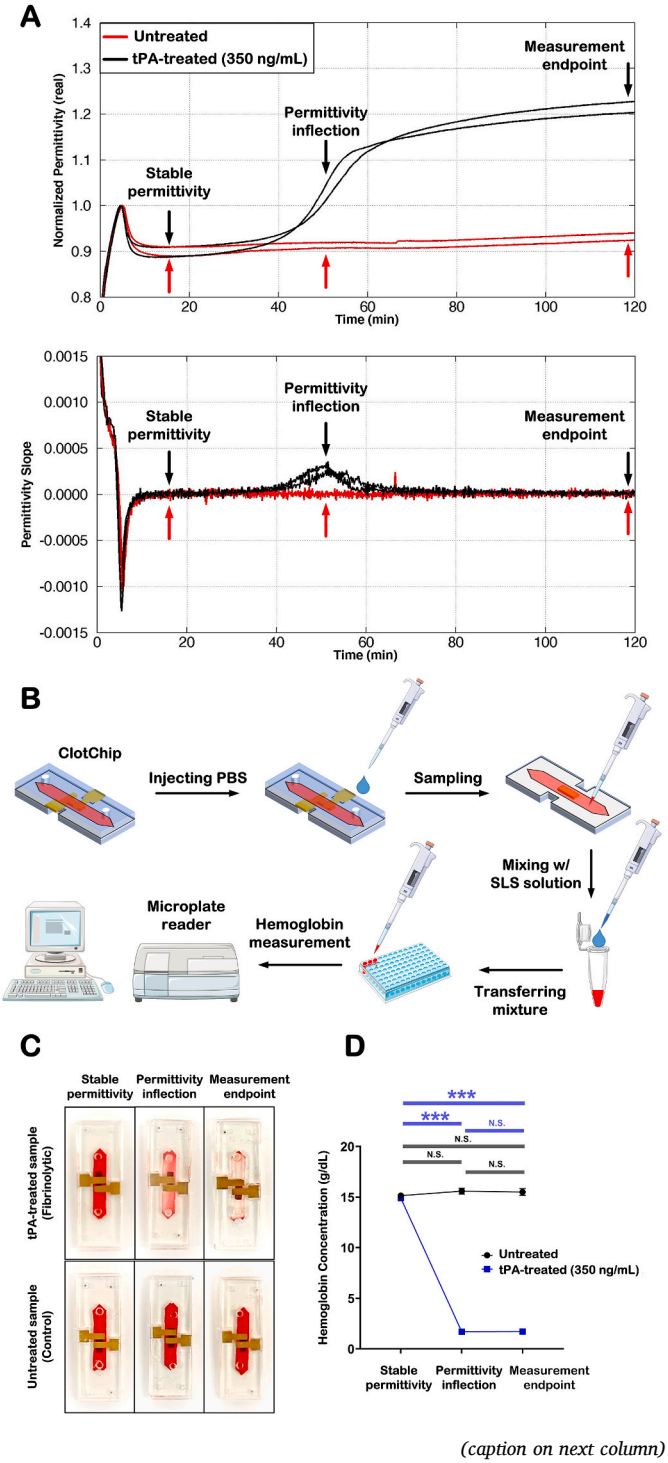

(caption on next column)

Fig. 3. Qualitative and quantitative analyses of fibrin clot stability inside the microfluidic channel in a fibrinolytic environment. **A)** ClotChip readout curve and its first derivative for an untreated whole blood sample as well as a sample treated with tPA at a concentration of 350 ng/mL. The samples had TF added to them at a concentration of 1 pg/mL. To assess fibrin clot stability, three different time points were selected on the readout curve corresponding to (i) when permittivity variation after T_{peak} had largely stabilized, (ii) fibrinolysis-induced permittivity inflection point on the tail end of the curve, and (iii) measurement endpoint. **B)** Illustration of the procedure for clot stability analysis at each of the three time points. First, 100 μL of phosphate-buffered saline (PBS) was injected into the ClotChip microfluidic channel. Next, 5 μL of the sample was collected from the microfluidic channel and mixed with sodium lauryl sulphate (SLS) solution. The mixture was then transferred to well plates for measuring the hemoglobin concentration of the mixture with a microplate reader. **C)** Visual observation of fibrin clots inside the ClotChip microfluidic channel at the three pre-defined time points after PBS injection. The tPA-treated (fibrinolytic) sample showed a stable clot at the first time point, with PBS unable to enter the microfluidic channel from the inlet port. By the time point of permittivity inflection, the fibrin clot had mostly dissolved and washed away after PBS injection. By the measurement endpoint, the microfluidic channel was devoid of any blood. In contrast, the untreated (control) sample maintained a stable clot throughout the 2-h duration of this experiment, with no sign of the clot dissolving and washing away after PBS injection. **D)** Output of microplate reader for hemoglobin measurements was in very good agreement with the visual observation of fibrin clots in **C**. Error bars are presented as mean ± SEM of three measurements for each untreated and tPA-treated sample at each time point.

4. Discussion

Timely diagnosis of hyperfibrinolysis with conventional assays is typically achieved using viscoelastometry instruments such as TEG or ROTEM. In ROTEM, hyperfibrinolysis is indicated when maximum lysis in an EXTEM or INTEM test is >15% and when the APTEM test results in rescued clot stability (Theusinger et al., 2011). The cost of performing parallel EXTEM, INTEM, and APTEM tests is $45. In TEG, hyperfibrinolysis is indicated by a 3–7.5% (or higher) elevation of the 30-min fibrinolysis (LY30) parameter (Chapman et al., 2013). The cost of a TEG 6s cartridge is $85.

In comparison, the fabrication cost of ClotChip can be considerably less than the related costs of TEG/ROTEM. The material costs of the PMMA plastic substrates and the DSA film are less than $0.10 combined. The gold ink costs $70 per gram. We have been able to produce >100 ClotChip sensors per gram of gold ink in real-world conditions, which include material waste and an estimated yield of ~90%. Thus, the total material cost for ClotChip fabrication can be < $1 per sensor.

Reader equipment costs can also be less expensive for ClotChip. Werfen's modern ROTEM Delta system costs $43,000. A TEG 6s similarly costs $42,000. The Agilent impedance analyzer used in this study was purchased for $16,000. Moreover, the impedance analyzer can be miniaturized into a more cost-effective and portable device using a low-cost embedded microprocessor and electronic circuitry customized to the operation frequency and signal range of the ClotChip sensor (Bakhshiani et al., 2016). We expect that a commercial ClotChip reader could cost < $2000.

Moreover, the cartridge shelf life of an assay is typically limited by the reagent used in the assay and may require special storage conditions. Since the ClotChip sensor is based on stable materials such as PMMA and gold, and it does not utilize any chemical reagents in its operation, we expect that a commercial ClotChip cartridge could have shelf life of >24 months stored at room temperature. In comparison, TEG 6s cartridges have a shelf life of 24 months stored at 2–8 °C, and ROTEM reagents have an unopened shelf life of 12 months stored at 2–8 °C.

As an electronic, label-free assay with a single disposable cartridge using a minuscule amount of whole blood, we envision ClotChip as a clinical decision support system that can be performed cost-effectively at the POC/POI, with potential to guide patient care in defined scenarios

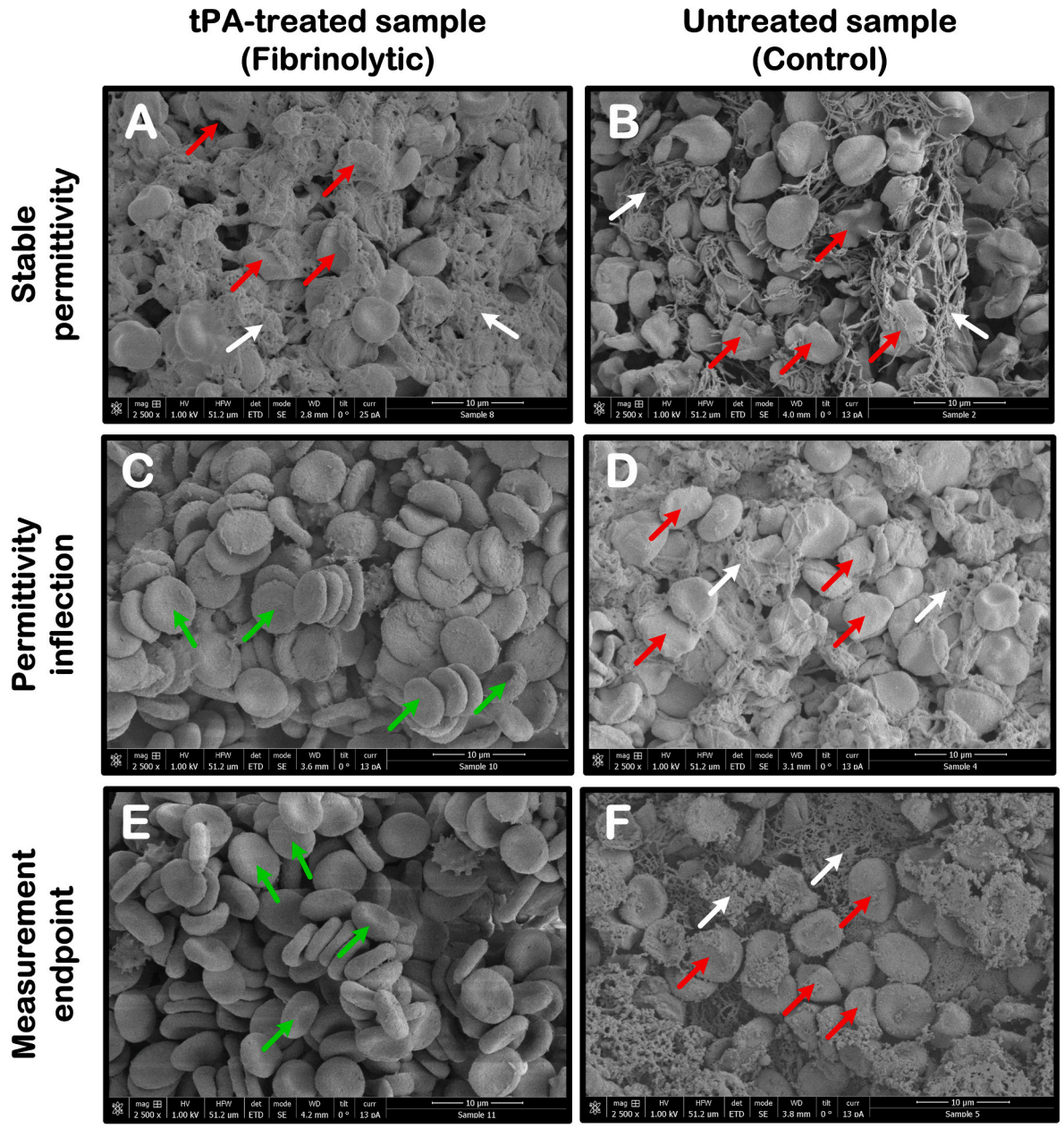

Fig. 4. Scanning electron microscope (SEM) images of fibrin clots for tPA-treated (fibrinolytic) and untreated (control) samples at three different time points on the ClotChip readout curve indicated in Fig. 3. **A–B)** Both samples formed stable clots as indicated by the deformation of red blood cells (RBCs) and their trapping in a netted fibrin mesh by the time the permittivity variation had stabilized. **C–D)** By the time point of permittivity inflection, the fibrin mesh had broken down in the fibrinolytic sample due to tPA-induced upregulated fibrinolysis, with the RBCs largely retrieving their biconcave disk-like shape. These changes were not observed in the control sample. **E–F)** By the measurement endpoint, the fibrin mesh had fully dissolved in the fibrinolytic sample, whereas the control sample continued to maintain a stable clot. The arrows point to the presence of the fibrin mesh (white) as well as examples of biconcave disk-like RBCs (green) and severely deformed RBCs (red).

with fibrinolysis-related hemostatic abnormalities. Such scenarios can include the measurement of increased fibrinolytic activity, e.g., in trauma, surgery, post-partum hemorrhage, and liver cirrhosis for the clinicians to decide whether to treat bleeding with antifibrinolytic drugs or not. Such scenarios can also include the detection of impaired fibrinolysis in venous and/or arterial thrombosis for the clinicians to decide on the duration of anticoagulation therapy that is administered.

Our future work will focus on clinical evaluation of the ClotChip sensor using blood samples from patients in above-mentioned scenarios to validate our findings and investigate the sensitivity of our assay. We also plan to evaluate blood samples from patients on antifibrinolytic drugs and those receiving tPA to optimize the high and low ends of our assay readings. Ultimately, the establishment of reference ranges of *normal* fibrinolytic parameters and subsequent establishment of deviation from normal reference ranges and statistical analyses of variance for *abnormal* fibrinolytic parameters in appropriate patient cohorts will enable the development of automated algorithms as part of a standard operating procedure to implement our assay clinically.

5. Conclusions

In this work, we presented a microfluidic dielectric sensor – termed ClotChip – for rapid assessment of the fibrinolytic status in whole blood. The sensor was shown to measure the real part of the blood dielectric

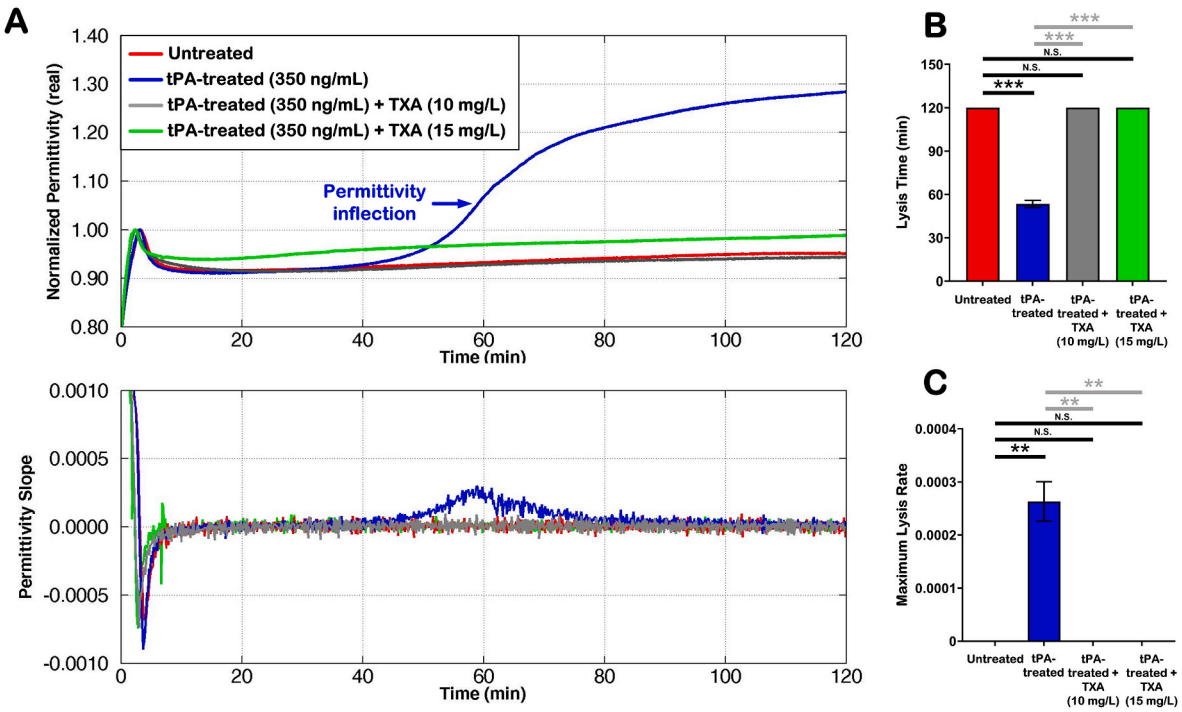

Fig. 5. Assessment of tranexamic acid (TXA) effect on upregulated fibrinolysis. **A)** ClotChip readout curve and its first derivative for an untreated whole blood sample, a sample treated with tPA at a concentration of 350 ng/mL, and the same tPA-treated sample with the addition of TXA at two different concentrations to inhibit the tPA-induced upregulated fibrinolysis. All samples had TF added to them at a concentration of 1 pg/mL. The ClotChip **B)** LT and **C)** MLR parameters could detect the correction in hemostatic function that occurred with TXA addition. In the absence of fibrin clot lysis within the 2-h duration of these experiments for the untreated and TXA-treated samples, a value of 120 min was assigned to LT for plotting the data. Error bars are presented as mean ± SEM of duplicate measurements.

permittivity in a frequency range of 10 kHz–100 MHz, with its readout curve defined as the temporal variation of the permittivity at 1 MHz as the sample underwent coagulation. Two different parameters in the ClotChip readout curve, LT and MLR, were shown to provide distinct information related to the time and rate of fibrin clot lysis, respectively, in a tPA-induced fibrinolytic environment. The ClotChip LT parameter exhibited a very strong positive correlation ($r \cong 0.96, p < 0.0001, n = 9$) to the ROTEM LT parameter, while the ClotChip MLR parameter showed a strong positive correlation ($r \cong 0.74, p < 0.05, n = 9$) to the ROTEM CLR parameter. In addition to being sensitive to the detection of tPA-induced upregulated fibrinolysis, the ClotChip sensor was shown to be able to detect the correction of hemostatic function mediated by the addition of TXA to inhibit dysregulated fibrinolysis. This work establishes the significant potential of ClotChip as a DS platform for rapid assessment of the fibrinolytic status at POC/POI using <10 μL of whole blood.

CRediT authorship contribution statement

Sina Pourang: Conceptualization, Methodology, Experimentation (ClotChip sensor fabrication and measurements), Data acquisition and analysis, Writing, Visualization. **Ujjal D.S. Sekhon:** Methodology, Experimentation (ROTEM and Hb concentration measurements), Data acquisition. **Dante Disharoon:** Methodology, Writing. **Sanjay P. Ahuja:** Conceptualization, Clinical guidance, Funding acquisition. **Michael A. Suster:** Conceptualization, Formal analysis, and interpretation, Validation, Supervision, Project administration, Funding acquisition. **Anirban Sen Gupta:** Conceptualization, Formal analysis, and interpretation, Validation, Resources, Supervision, Project administration, Funding acquisition. **Pedram Mohseni:** Conceptualization, Formal analysis, and interpretation, Validation, Resources, Writing, Visualization, Supervision, Project administration, Funding acquisition.

Declaration of competing interest

The authors declare the following financial interests/personal relationships which may be considered as potential competing interests: M. A. Suster and P. Mohseni are inventors of intellectual property related to this study that has been licensed by Case Western Reserve University to XaTek Inc. They report research funding, consulting fees, and royalties from XaTek Inc. during the conduct of this study. S. P. Ahuja reports research funding from XaTek Inc. and fees from Bayer, Sanofi, Novo Nordisk, and Takeda. A. Sen Gupta is a co-founder of Haima Therapeutics and an inventor on patents regarding hemostatic therapeutic technologies that are licensed to Haima Therapeutics. S. Pourang, U. D. S. Sekhon, and D. Disharoon report no conflict.

Acknowledgements

This work is supported by the US Army Medical Research and Development Command under Contract No. W81XWH20C0120, National Institutes of Health (NIH) under Award No. R01HL121212, Case-Coulter Translational Research Partnership program at Case Western Reserve University, and the NIH Center for Accelerated Innovations at Cleveland Clinic. The views, opinions and/or findings contained in this manuscript are those of the authors and should not be construed as an official Department of the Army position, policy or decision unless so designated by other documentation.

Appendix A. Supplementary data

Supplementary data to this article can be found online at https://doi.org/10.1016/j.bios.2022.114299.

References

Asami, K., Sekine, K., 2007. Dielectric modeling of erythrocyte aggregation in blood. J. Phys. D Appl. Phys. 40, 2197–2204. https://doi.org/10.1088/0022-3727/40/7/051.

Bakhshiani, M., Suster, M.A., Mohseni, P., 2016. A palmtop platform for miniaturized dielectric spectroscopy from MHz to GHz. Proc. IEEE Int. New Circ. Syst. (NEWCAS) Conf. https://doi.org/10.1109/NEWCAS.2016.7604805.

Brill, J.B., Brenner, M., Duchesne, J., Roberts, D., Ferrada, P., Horer, T., Kauvar, D., Khan, M., Kirkpatrick, A., Ordonez, C., Perreira, B., Priouzram, A., Cotton, B.A., 2021. The role of TEG and ROTEM in damage control resuscitation. Shock 56, 52–61. https://doi.org/10.1097/SHK.0000000000001686.

Brohi, K., Cohen, M.J., Ganter, M.T., Matthay, M.A., Mackersie, R.C., Pittet, J.F., 2007. Acute traumatic coagulopathy: initiated by hypoperfusion: modulated through the protein C pathway? Ann. Surg. 245, 812–818. https://doi.org/10.1097/01.sla.0000256862.79374.31.

Cakmak, O., Ermek, E., Kilinc, N., Bulut, S., Baris, I., Kavakli, I.H., Yaralioglu, G.G., Urey, H., 2015. A cartridge based sensor array platform for multiple coagulation measurements from plasma. Lab Chip 15, 113–120. https://doi.org/10.1039/c4lc00809j.

Chapman, M.P., Moore, E.E., Moore, H.B., Gonzalez, E., Gamboni, F., Chandler, J.G., Mitra, S., Ghasabyan, A., Chin, T.L., Sauaia, A., Banerjee, A., Silliman, C.C., 2016. Overwhelming tPA release, not PAI-1 degradation, is responsible for hyperfibrinolysis in severely injured trauma patients. J. Trauma Acute Care Surg. 80, 16–25. https://doi.org/10.1097/TA.0000000000000885.

Chapman, M.P., Moore, E.E., Ramos, C.R., Ghasabyan, A., Harr, J.N., Chin, T.L., Stringham, J.R., Sauaia, A., Silliman, C.C., Banerjee, A., 2013. Fibrinolysis greater than 3% is the critical value for initiation of antifibrinolytic therapy. J. Trauma Acute Care Surg. 75, 961–967. https://doi.org/10.1097/TA.0b013e3182aa9c9f.

Chen, D., Song, S., Ma, J., Zhang, Z., Wang, P., Liu, W., Guo, Q., 2017. Micro-electromechanical film bulk acoustic sensor for plasma and whole blood coagulation monitoring. Biosens. Bioelectron. 91, 465–471. https://doi.org/10.1016/j.bios.2016.12.063.

Cotton, B.A., Harvin, J.A., Kostousouv, V., Minei, K.M., Radwan, Z.A., Schöchl, H., Wade, C.E., Holcomb, J.B., Matijevic, N., 2012. Hyperfibrinolysis at admission is an uncommon but highly lethal event associated with shock and prehospital fluid administration. J. Trauma Acute Care Surg. 73, 365–370. https://doi.org/10.1097/TA.0b013e31825c1234.

Diamond, S.L., Rossi, J.M., 2021. Point of care whole blood microfluidics for detecting and managing thrombotic and bleeding risks. Lab Chip 21, 3667–3674. https://doi.org/10.1039/d1lc00465d.

Görlinger, K., Dirkmann, D., Hanke, A.A., 2021. Rotational thromboelastometry (ROTEM®). In: Moore, H.B., Neal, M.D., Moore, E.E. (Eds.), Trauma Induced Coagulopathy. Springer, Cham. https://doi.org/10.1007/978-3-030-53606-0_18.

Harder, S., dos Santos, S.M., Krozer, V., Moll, J., 2019. Surface acoustic wave-based microfluidic coagulation device for monitoring anticoagulant therapy. Semin. Thromb. Hemost. 45, 253–258. https://doi.org/10.1055/s-0038-1676318.

Hartmann, J., Murphy, M., Dias, J.D., 2020. Viscoelastic hemostatic assays: moving from the laboratory to the site of care—a review of established and emerging technologies. Diagnostics 10, 1–14. https://doi.org/10.3390/diagnostics10020118.

Hayashi, Y., Brun, M.A., Machida, K., Nagasawa, M., 2015. Principles of dielectric blood coagulometry as a comprehensive coagulation test. Anal. Chem. 87, 10072–10079. https://doi.org/10.1021/acs.analchem.5b02723.

Hayashi, Y., Katsumoto, Y., Omori, S., Yasuda, A., Asami, K., Kaibara, M., Uchimura, I., 2010. Dielectric coagulometry: a new approach to estimate venous thrombosis risk. Anal. Chem. 82, 9769–9774. https://doi.org/10.1021/ac101927n.

Hayashi, Y., Oshige, I., Katsumoto, Y., Omori, S., Yasuda, A., Asami, K., 2008. Dielectric inspection of erythrocyte morphology. Phys. Med. Biol. 53, 2553–2564. https://doi.org/10.1088/0031-9155/53/10/007.

Jain, A., Graveline, A., Waterhouse, A., Vernet, A., Flaumenhaft, R., Ingber, D.E., 2016. A shear gradient-activated microfluidic device for automated monitoring of whole blood haemostasis and platelet function. Nat. Commun. 7, 1–10. https://doi.org/10.1038/ncomms10176.

Katz, J., Lurie, A., Becker, D., Metz, J., 1970. The euglobulin lysis time test: an ineffectual monitor of the therapeutic inhibition of fibrinolysis. J. Clin. Pathol. (Lond.) 23, 529–532.

Kornblith, L.Z., Moore, H.B., Cohen, M.J., 2019. Trauma-induced coagulopathy: the past, present, and future. J. Thromb. Haemostasis 17, 852–862. https://doi.org/10.1111/jth.14450.

Kutcher, M.E., Cripps, M.W., McCreery, R.C., Crane, I.M., Greenberg, M.D., Cachola, L. M., Redick, B.J., Nelson, M.F., Cohen, M.J., 2012. Criteria for empiric treatment of hyperfibrinolysis after trauma. J. Trauma Acute Care Surg. 73, 87–93. https://doi.org/10.1097/TA.0b013e3182598c70.

Lei, K.F., Chen, K.H., Tsui, P.H., Tsang, N.M., 2013. Real-time electrical impedimetric monitoring of blood coagulation process under temperature and hematocrit variations conducted in a microfluidic chip. PLoS One 8, 1–7. https://doi.org/10.1371/journal.pone.0076243.

Li, D., Liu, X., Chai, Y., Shan, J., Xie, Y., Liang, Y., Huang, S., Zheng, W., Li, Z., 2022. Point-of-care blood coagulation assay enabled by printed circuit board-based digital microfluidics. Lab Chip. https://doi.org/10.1039/D1LC00981H.

Li, J., Wan, N., Wen, J., Cheng, G., He, L., Cheng, L., 2019. Quantitative detection and evaluation of thrombus formation based on electrical impedance spectroscopy. Biosens. Bioelectron. 141, 1–5. https://doi.org/10.1016/j.bios.2019.111437.

Maji, D., De La Fuente, M., Kucukal, E., Sekhon, U.D.S., Schmaier, A.H., Sen Gupta, A., Gurkan, U.A., Nieman, M.T., Stavrou, E.X., Mohseni, P., Suster, M.A., 2018. Assessment of whole blood coagulation with a microfluidic dielectric sensor. J. Thromb. Haemostasis 16, 2050–2056. https://doi.org/10.1111/jth.14244.

Maji, D., Nayak, L., Martin, J., Sekhon, U.D.S., Sen Gupta, A., Mohseni, P., Suster, M.A., Ahuja, S.P., 2019a. A novel, point-of-care, whole-blood assay utilizing dielectric spectroscopy is sensitive to coagulation factor replacement therapy in haemophilia A patients. Haemophilia 25, 885–892. https://doi.org/10.1111/hae.13799.

Maji, D., Opneja, A., Suster, M.A., Bane, K.L., Wilson, B.M., Mohseni, P., Stavrou, E.X., 2021. Monitoring DOACs with a novel dielectric microsensor: a clinical study. Thromb. Haemostasis 121, 58–69. https://doi.org/10.1055/s-0040-1715589.

Maji, D., Pourang, S., Sekhon, U.D.S., Sen Gupta, A., Suster, M.A., Mohseni, P., 2019b. Toward diagnosis of platelet loss in trauma injury using a microfluidic dielectric sensor. Proc. IEEE Sensors Conf. https://doi.org/10.1109/SENSORS43011.2019.8956491.

Maji, D., Suster, M.A., Kucukal, E., Sekhon, U.D.S., Sen Gupta, A., Gurkan, U.A., Stavrou, E.X., Mohseni, P., 2017. ClotChip: a microfluidic dielectric sensor for point-of-care assessment of hemostasis. IEEE Trans. Biomed. Circ. Syst. 11, 1459–1469. https://doi.org/10.1109/TBCAS.2017.2739724.

Mohammadi Aria, M., Erten, A., Yalcin, O., 2019. Technology advancements in blood coagulation measurements for point-of-care diagnostic testing. Front. Bioeng. Biotechnol. 7, 1–18. https://doi.org/10.3389/fbioe.2019.00395.

Moore, H.B., Moore, E.E., Gonzalez, E., Chapman, M.P., Chin, T.L., Silliman, C.C., Banerjee, A., Sauaia, A., 2014. Hyperfibrinolysis, physiologic fibrinolysis, and fibrinolysis shutdown: the spectrum of postinjury fibrinolysis and relevance to antifibrinolytic therapy. J. Trauma Acute Care Surg. 77, 811–817. https://doi.org/10.1097/TA.0000000000000341.

Oshiro, I., Takenaka, T., Maeda, J., 1982. New method for hemoglobin determination by using sodium lauryl sulfate (SLS). Clin. Biochem. 15, 83–88. https://doi.org/10.1016/S0009-9120(82)91069-4.

Picetti, R., Shakur-Still, H., Medcalf, R.L., Standing, J.F., Roberts, I., 2019. What concentration of tranexamic acid is needed to inhibit fibrinolysis? A systematic review of pharmacodynamics studies. Blood Coagul. Fibrinolysis 30, 1–10. https://doi.org/10.1097/MBC.0000000000000789.

Pourang, S., Maji, D., Sekhon, U.D.S., Sen Gupta, A., Suster, M.A., Mohseni, P., 2020. Monitoring fibrin polymerization effects on whole blood coagulation using a microfluidic dielectric sensor. Proc. IEEE Sensors Conf. https://doi.org/10.1109/SENSORS47125.2020.9278794.

Pourang, S., Suster, M.A., Mohseni, P., Nayak, L.V., 2021. Assessment of hypercoagulable state in whole blood in sepsis patients using a novel microfluidic dielectric sensor. Blood 138, 1882. https://doi.org/10.1182/blood-2021-149273.

Ramaswamy, B., Yeh, Y.T.T., Zheng, S.Y., 2013. Microfluidic device and system for point-of-care blood coagulation measurement based on electrical impedance sensing. Sensor. Actuator. B Chem. 180, 21–27. https://doi.org/10.1016/j.snb.2011.11.031.

Roberts, I., Shakur, H., Coats, T., Hunt, B., Balogun, E., Barnetson, L., Cook, L., Kawahara, T., Perel, P., Prieto-Merino, D., Ramos, M., Cairns, J., Guerriero, C., 2013. The CRASH-2 trial: a randomised controlled trial and economic evaluation of the effects of tranexamic acid on death, vascular occlusive events and transfusion requirement in bleeding trauma patients. Health Technol. Assess. 17, 1–80. https://doi.org/10.3310/hta17100.

Rossi, J.M., Diamond, S.L., 2020. Scalable manufacture of a disposable, storage-stable eight-channel microfluidic device for rapid testing of platelet, coagulation, and drug function under whole blood flow. Biomicrofluidics 14, 1–11. https://doi.org/10.1063/5.0023312.

Schoeman, R.M., Rana, K., Danes, N., Lehmann, M., Di Paola, J.A., Fogelson, A.L., Leiderman, K., Neeves, K.B., 2017. A microfluidic model of hemostasis sensitive to platelet function and coagulation. Cell. Mol. Bioeng. 10, 3–15. https://doi.org/10.1007/s12195-016-0469-0.

Sekar, P.K., Liang, X.M., Kahng, S.J., Shu, Z., Dichiara, A.B., Chung, J.H., Wu, Y., Gao, D., 2022. Simultaneous multiparameter whole blood hemostasis assessment using a carbon nanotube-paper composite capacitance sensor. Biosens. Bioelectron. 197, 1–10. https://doi.org/10.1016/j.bios.2021.113786.

Sweeney, R.E., Nguyen, V., Alouidor, B., Budiman, E., Wong, R.K., Yoon, J.Y., 2019. Flow rate and Raspberry Pi-based paper microfluidic blood coagulation assay device. IEEE Sensor. J. 19, 4743–4751. https://doi.org/10.1109/JSEN.2019.2902065.

Theusinger, O.M., Wanner, G.A., Emmert, M.Y., Billeter, A., Eismon, J., Seifert, B., Simmen, H.P., Spahn, D.R., Baulig, W., 2011. Hyperfibrinolysis diagnosed by rotational thromboelastometry (ROTEM®) is associated with higher mortality in patients with severe trauma. Anesth. Analg. 113, 1003–1012. https://doi.org/10.1213/ANE.0b013e31822e183f.

Williams, N.X., Carroll, B., Noyce, S.G., Hobbie, H.A., Joh, D.Y., Rogers, J.G., Franklin, A. D., 2021. Fully printed prothrombin time sensor for point-of-care testing. Biosens. Bioelectron. 172, 1–10. https://doi.org/10.1016/j.bios.2020.112770.

Xu, S., Piao, J., Lee, B., Lim, C., Shin, S., 2020. Platelet thrombus formation by upstream activation and downstream adhesion of platelets in a microfluidic system. Biosens. Bioelectron. 165, 1–8. https://doi.org/10.1016/j.bios.2020.112395.